May. 12th, 2023

Star Formation Newsletter No. 361 #17-32

Shota Notsu (Dept. of Astronomy, Univ. of Tokyo)

ALMA Cycle 10プロポーザル お疲れ様でした！

17. **Cyanopolyyne chemistry in the L1544 prestellar core: new insights from GBT observations**

Eleonora Bianchi, Anthony Remijan, Claudio Codella, Cecilia Ceccarelli, Francois Lique, Silvia Spezzano, Nadia Balucani, Paola Caselli, Eric Herbst, Linda Podio, Charlotte Vastel, Brett McGuire

★ We report a comprehensive study of the cyanopolyyne chemistry in the prototypical prestellar core L1544. Using the 100m Robert C. Byrd Green Bank Telescope (GBT) we observe 3 emission lines of HC_3N, 9 lines of HC_5N, 5 lines of HC_7N, and 9 lines of HC_9N. HC_9N is detected for the first time towards the source. The high spectral resolution ($\sim$ 0.05 km s^{-1}) reveals double-peak spectral line profiles with the redshifted peak a factor 3-5 brighter. Resolved maps of the core in other molecular tracers indicates that the southern region is redshifted. Therefore, the bulk of the cyanopolyyne emission is likely associated with the southern region of the core, where free carbon atoms are available to form long chains, thanks to the more efficient illumination of the interstellar field radiation. We perform a simultaneous modelling of the HC_5N, HC_7N, and HC_9N lines, to investigate the origin of the emission. To enable this analysis, we performed new calculation of the collisional coefficients. The simultaneous fitting indicates a gas kinetic temperature of 5–12 K, a source size of 80 arcsec, and a gas density larger than 100 cm^{-3}. The HC_5N:HC_7N:HC_9N abundance ratios measured in L1544 are about 1:6:4. We compare our observations with those towards the the well-studied starless core TMC-1 and with the available measurements in different star-forming regions. The comparison suggests that a complex carbon chain chemistry is active in other sources and it is related to the presence of free gaseous carbon. Finally, we discuss the possible formation and destruction routes in the light of the new observations.

Green Bank Telescopeでprestellar core L1544に対し、HC_3N, HC_5N, HC_7N, HC_9Nの複数輝線をそれぞれ検出。
速度プロファイルの解析から、南側の領域に偏って分布
TMC-1等の他の星なしコア天体の観測結果とも比較し、carbon-chain chemistry activeと議論

https://arxiv.org/abs/2301.10106v2

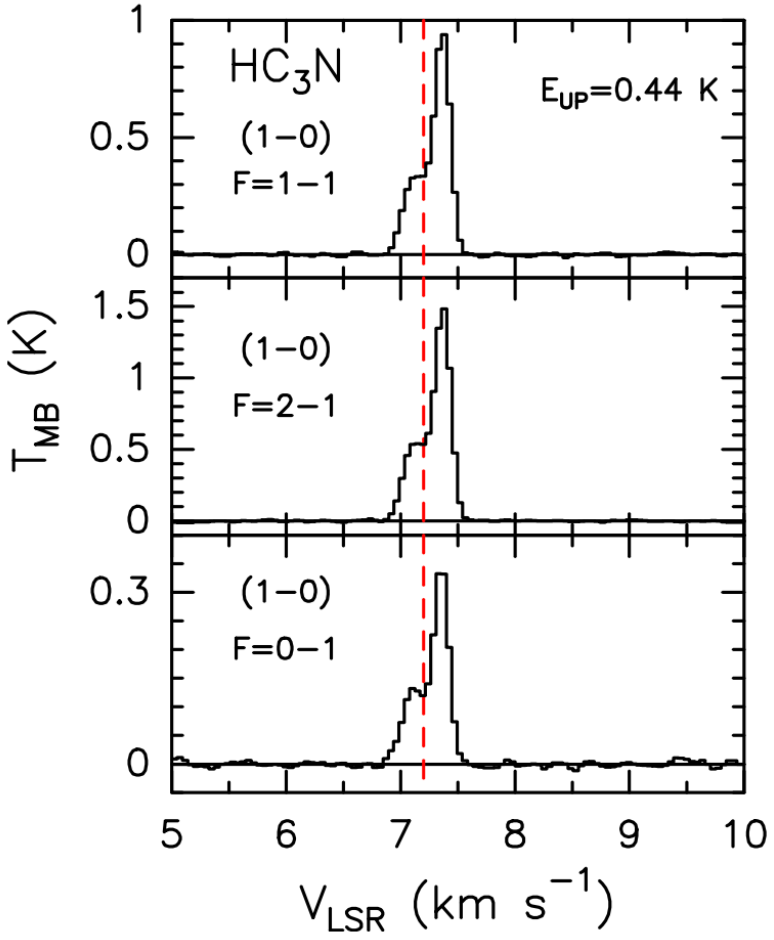

Figure 1. HC_3N transitions observed towards L1544 with the GBT. The vertical dashed lines mark the ambient LSR velocity (+ 7.2 km s^{-1}, Tafalla et al. 1998). The upper level energy of each transition is reported on the right inside the top panel.

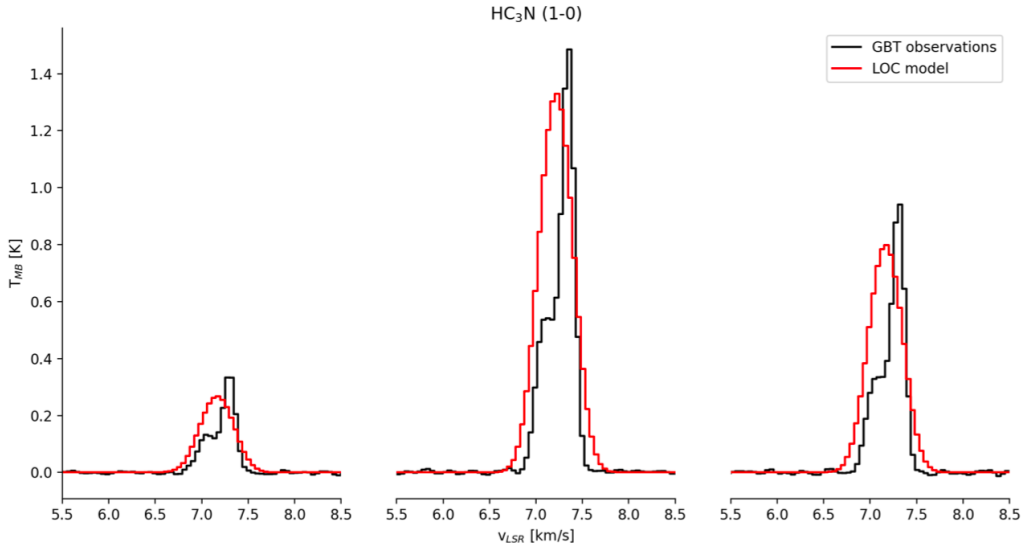

Figure 5. Comparison between the observed HC_3N line profiles and the theoretical profiles predicted using the radiative transfer code LOC (see Sect. 3.1). The model, assuming spherical symmetry distribution, reproduce the line intensities but not the shape of the profiles. This suggests an asymmetric distribution of cyanopolyynes across the core, with the red-shifted component brighter than the blue-shifted one.

赤線：対称分布のモデル
黒線：観測

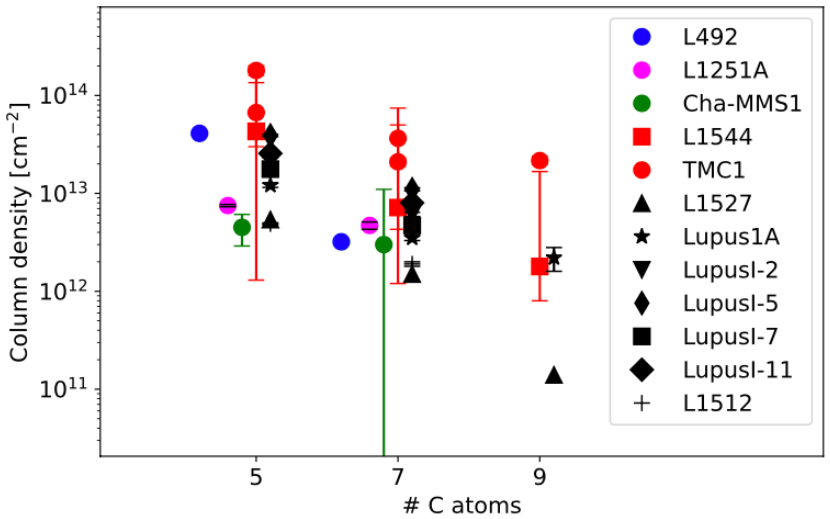

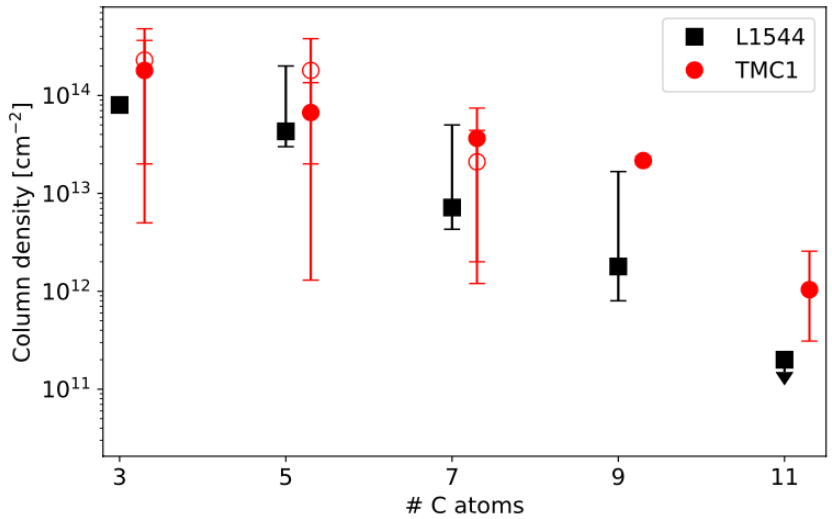

Star forming region	Source	T_{ex} K	$N(HC_5N)$ 10^{12} cm^{-2}	$N(HC_7N)$ 10^{12} cm^{-2}	$N(HC_9N)$ 10^{12} cm^{-2}	References
Taurus	TMC-1	8	66.9 (1.3)	36.5 (1.3)	22 (2)	[1]
Taurus	TMC-1	8.6 (0.2) – 7.6 (0.2)	180 (20)	21 (2)	–	[2,3]
Taurus	L1527 IRAS 04368+2557	12.3	5.4	1.5	0.14	[4]
Lupus	Lupus-1A	10.0 (0.2)	12.1 (0.6)	3.5 (0.2)	2.2 (0.6)	[5,6,7]
Serpens	Serpens South 1a	7	12 (1)	6.0 (0.2)	3.1 (0.2)	[8]
Lupus	LupusI-2	11.5 (0.2)	22 (1)	6.1 (0.3)	–	[7]
Lupus	LupusI-5	11.2 (0.1)	39 (1)	11.0 (0.4)	–	[7]
Lupus	LupusI-7/8/9	10.2 (0.1)	17.7 (0.6)	4.7 (0.2)	–	[7]
Lupus	LupusI-11	11.9 (0.8)	25.6 (0.8)	8.0 (0.3)	–	[7]
Chameleon	Cha-MMS1	7 (1)	4.5 (1.6)	3 (8)	–	[9]
Taurus-Auriga	L1512	8.7 (0.7)	4.9 (0.1)	1.9 (0.1)	–	[10]
Cepheus	L1251A	6.2 (0.3)	7.5 (0.2)	4.7 (0.4)	–	[10]
Aquila Rift	L492	6.5–10	41	3.2	–	[11]

Table 3. Cyanopolyynes abundances in starless cores. [1] Loomis et al. 2021; [2] Cernicharo et al. 2020; [3] Cabezas et al. 2022 ; [4] Sakai et al. 2008; [5] Sakai et al. 2009; [6] Sakai et al. 2010; [7] Wu et al. 2019; [8] Li et al. 2016; [9] Cordiner et al. 2012; [10] Cordiner et al. 2011; [11] Hirota & Yamamoto 2006.

C l richな領域
→炭素鎖分子の生成が進む

今回の天体
年齢若くCO形成前
or
UV/CRが強くCO破壊

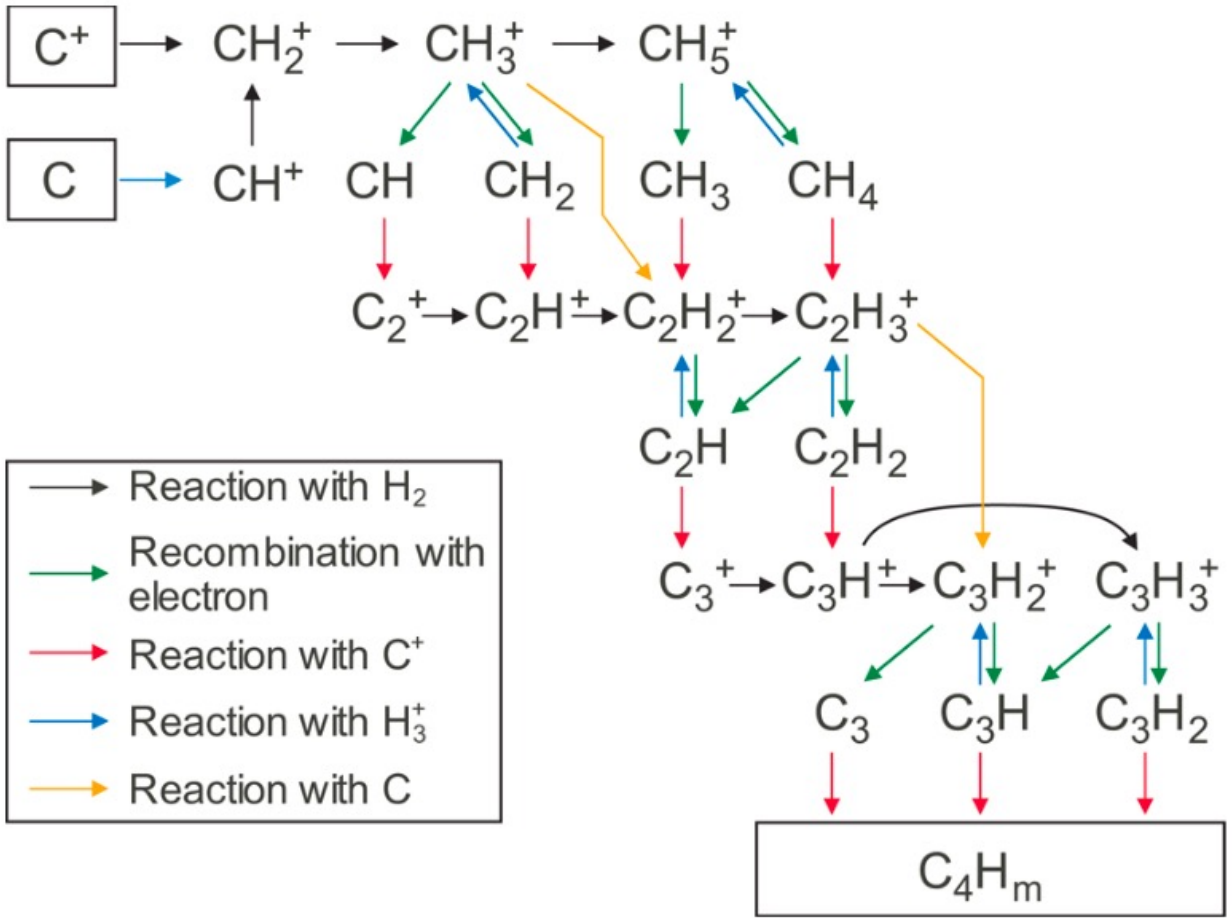

Figure from Sakai & Yamamato (2013)

29. **Molecular Mapping of DR Tau's Protoplanetary Disk, Envelope, Outflow, and Large-Scale Spiral Arm**

Jane Huang, Edwin A. Bergin, Jaehan Bae, Myriam Benisty, Sean M. Andrews

★ DR Tau has been noted for its unusually high variability in comparison with other T Tauri stars. Although it is one of the most extensively studied pre-main sequence stars, observations with millimeter interferometry have so far been relatively limited. We present NOEMA images of ^{12}CO, ^{13}CO, $C^{18}O$, SO, DCO^+, and H_2CO toward DR Tau at a resolution of $\sim 0.5''$ ($\sim$ 100 au). In addition to the protoplanetary disk, CO emission reveals an envelope, a faint asymmetric outflow, and a spiral arm with a clump. The $\sim$ 1200 au extent of the CO arm far exceeds that of the spiral arms previously detected in scattered light, which underlines the necessity of sensitive molecular imaging for contextualizing the disk environment. The kinematics and compact emission distribution of $C^{18}O$, SO, DCO^+, and H_2CO indicate that they originate primarily from within the Keplerian circumstellar disk. The SO emission, though, also exhibits an asymmetry that may be due to interaction with infalling material or unresolved substructure. The complex environment of DR Tau is reminiscent of those of outbursting FUor sources and some EXor sources, suggesting that DR Tau's extreme stellar activity could likewise be linked to disk instabilities promoted by large-scale infall.

活動性の高いT Tauri星 DR Tauの分子輝線をNOEMAで観測 (0.5''=100 au分解能)
12CO: 1200au 程度まで広がっており、エンベロープ, わずかに非軸対称性のあるアウトフロー, 渦状腕を検出

$C^{18}O$, SO, DCO^+, HCO^+ → Kepler円盤, SOの非対称性は未検出の構造か降着流との相互作用を反映

https://arxiv.org/abs/2301.02674v1

Table 1. Imaging Summary for Primary Line Targets

Transition	Synthesized beam (arcsec × arcsec (°))	Per-channel RMS noise[a] (mJy beam^{-1})	Velocity range[b] (km s^{-1})	Extraction Mask Diameter (arcsec)	Flux[c] (mJy km s^{-1})
^{12}CO $J = 2 - 1$	0.79 × 0.47 (18.2°)	7	$[-2, 17]$	21	37900 ± 200[d]
^{13}CO $J = 2 - 1$	0.84 × 0.49 (17.3°)	6	$[7.6, 11.4]$	21	5730 ± 70[d]
C^{18}O $J = 2 - 1$	0.85 × 0.50 (17.3°)	6	$[9.0, 10.8]$	4	622 ± 10
SO $J_N = 6_5 - 5_4$	0.85 × 0.50 (17.2°)	6	$[9.0, 10.8]$	3	195 ± 9
SO $J_N = 5_5 - 4_4$	0.86 × 0.50 (17.1°)	6	$[9.0, 10.8]$	3	96 ± 10
DCO$^+$ $J = 3 - 2$	0.86 × 0.50 (17.1°)	6	$[9.0, 10.8]$	3	40 ± 10
H_2CO $J_{K_aK_c} = 3_{03} - 2_{02}$	0.86 × 0.50 (17.2°)	6	$[9.0, 10.8]$	3	248 ± 11
H_2CO $J_{K_aK_c} = 3_{22} - 2_{21}$	1.20 × 0.93 (17.1°)	7	$[9.0, 10.8]$	3	< 30
H_2CO $J_{K_aK_c} = 3_{21} - 2_{20}$	1.20 × 0.93 (17.1°)	7	$[9.0, 10.8]$	3	38 ± 8

[a] With channel widths of 0.2 km s^{-1}.

[b] LSRK velocity range over which moment maps are produced and the flux is estimated.

[c] The 1σ error bars do not include the systematic flux uncertainty ($\sim 10\%$).

[d] These lines are significantly affected by spatial filtering, so the statistical uncertainty does not reflect the true uncertainty in the fluxes.

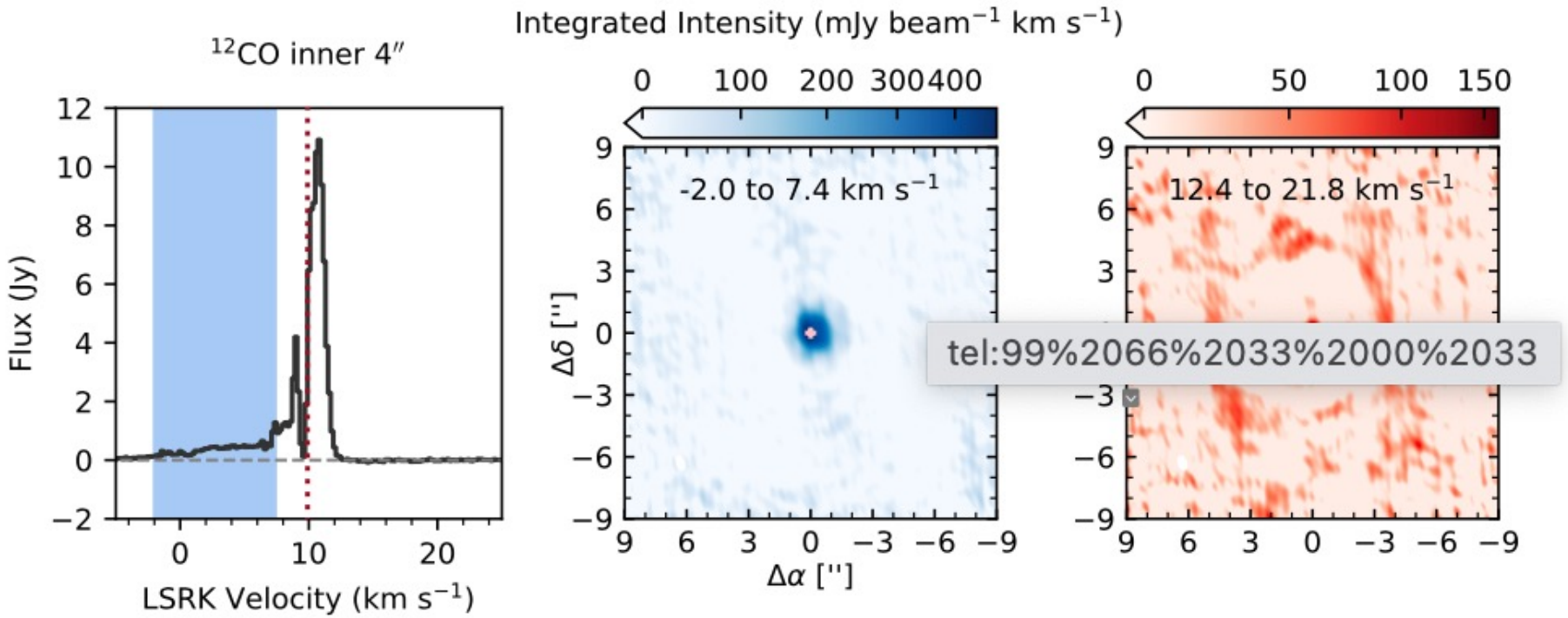
Integrated Intensity (mJy beam^{-1} km s^{-1})
^{12}CO inner 4″
Flux (Jy)
LSRK Velocity (km s^{-1})
-2.0 to 7.4 km s^{-1}
12.4 to 21.8 km s^{-1}
Δδ ['']
Δα ['']
tel:99%2066%2033%2000%2033

速度で切り分け

Envelope & Outflows→

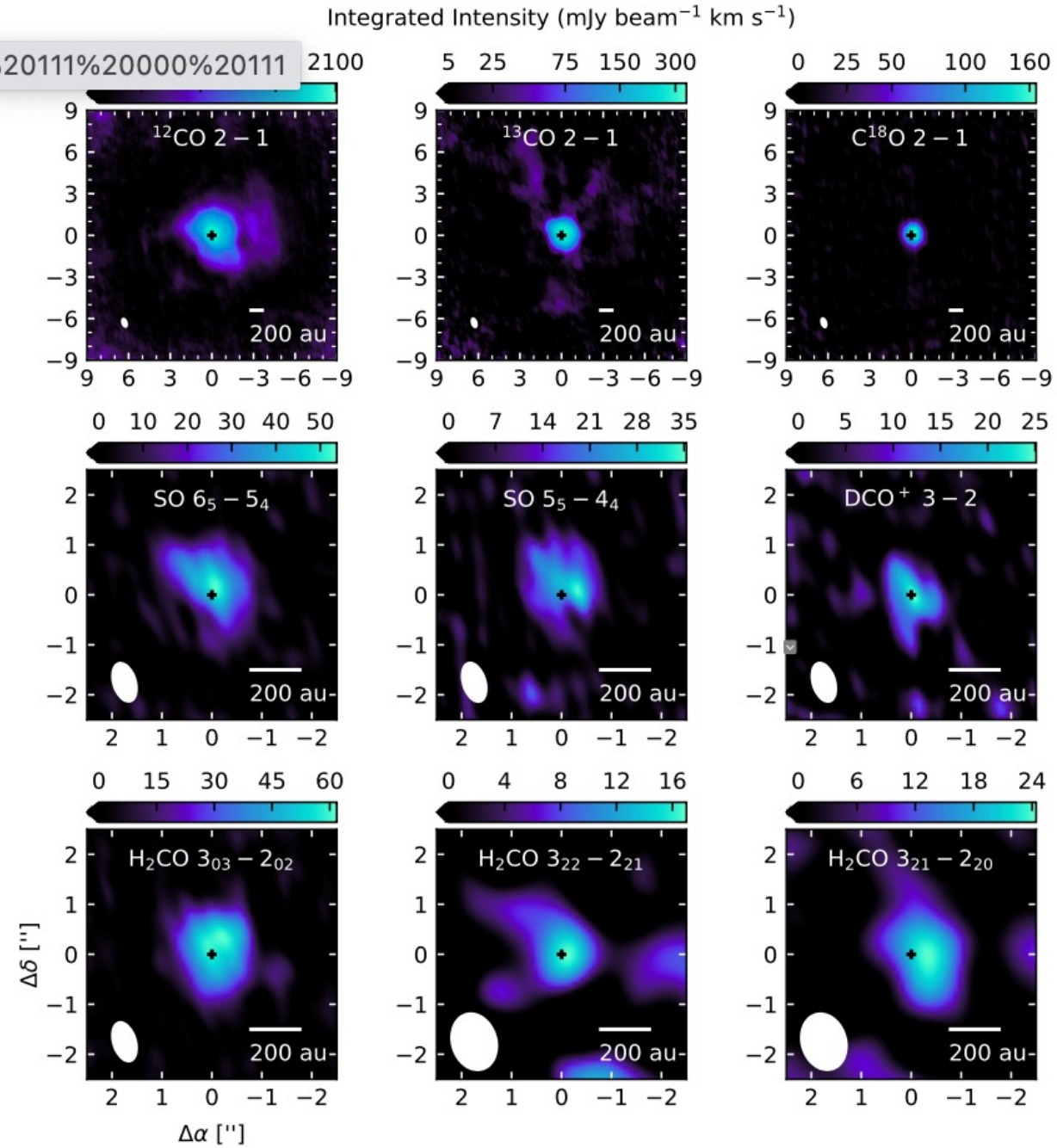

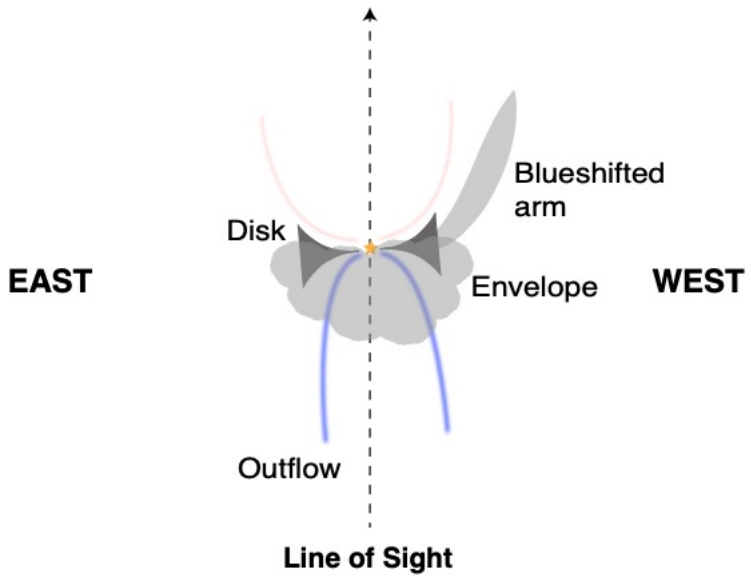
EAST
Disk
Blueshifted arm
Envelope
WEST
Outflow
Line of Sight

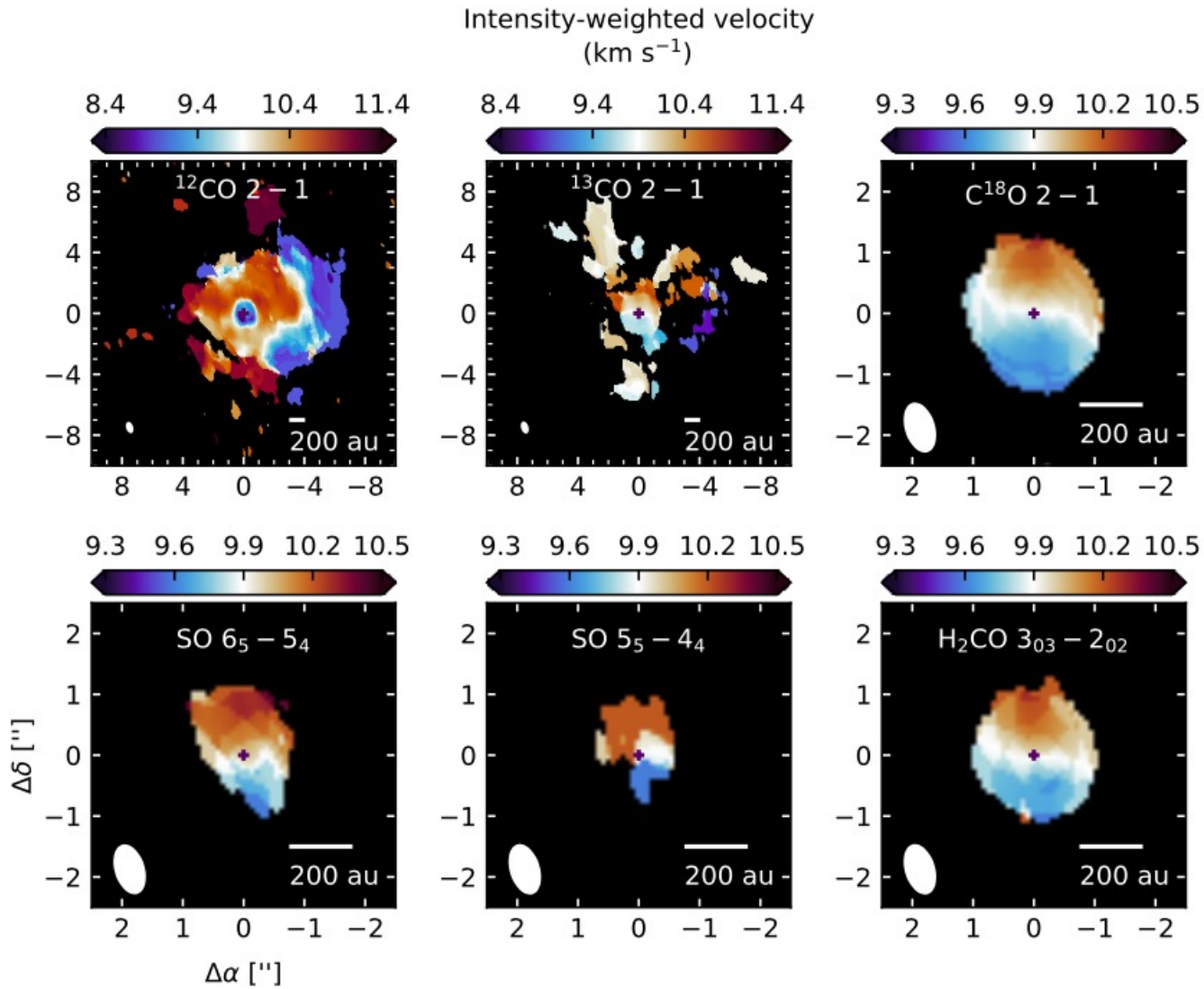
Intensity-weighted velocity (km s^{-1})
^{12}CO 2 – 1
^{13}CO 2 – 1
C^{18}O 2 – 1
SO $6_5 - 5_4$
SO $5_5 - 4_4$
H_2CO $3_{03} - 2_{02}$
200 au
Δδ ['']
Δα ['']

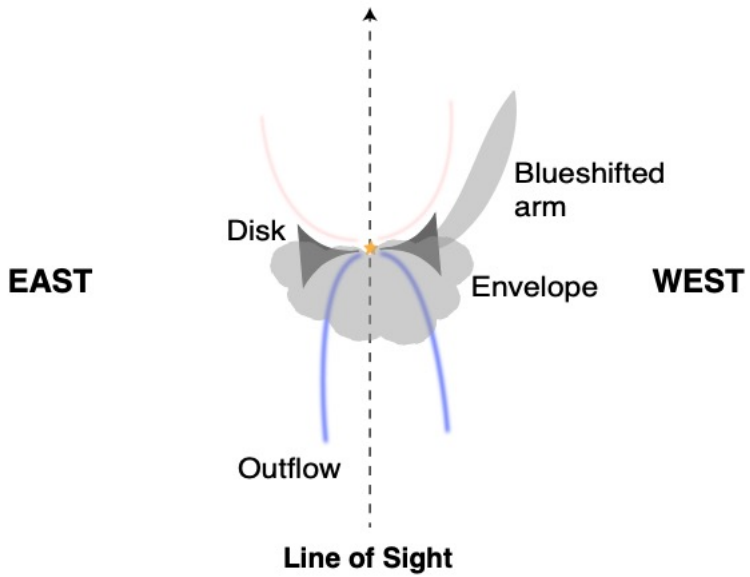
EAST
WEST
Disk
Blueshifted arm
Envelope
Outflow
Line of Sight

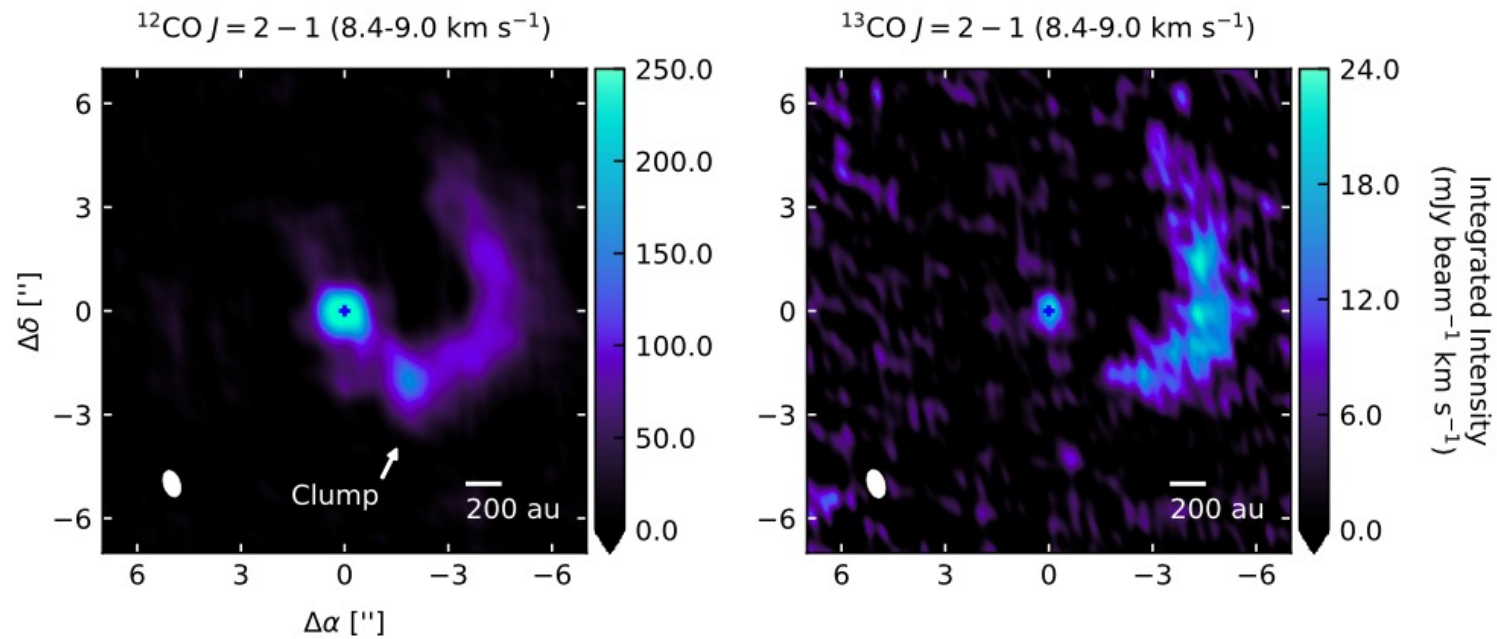
^{12}CO $J = 2 - 1$ (8.4-9.0 km s^{-1})
^{13}CO $J = 2 - 1$ (8.4-9.0 km s^{-1})
Clump
200 au
Δδ ['']
Δα ['']
Integrated Intensity (mJy beam^{-1} km s^{-1})

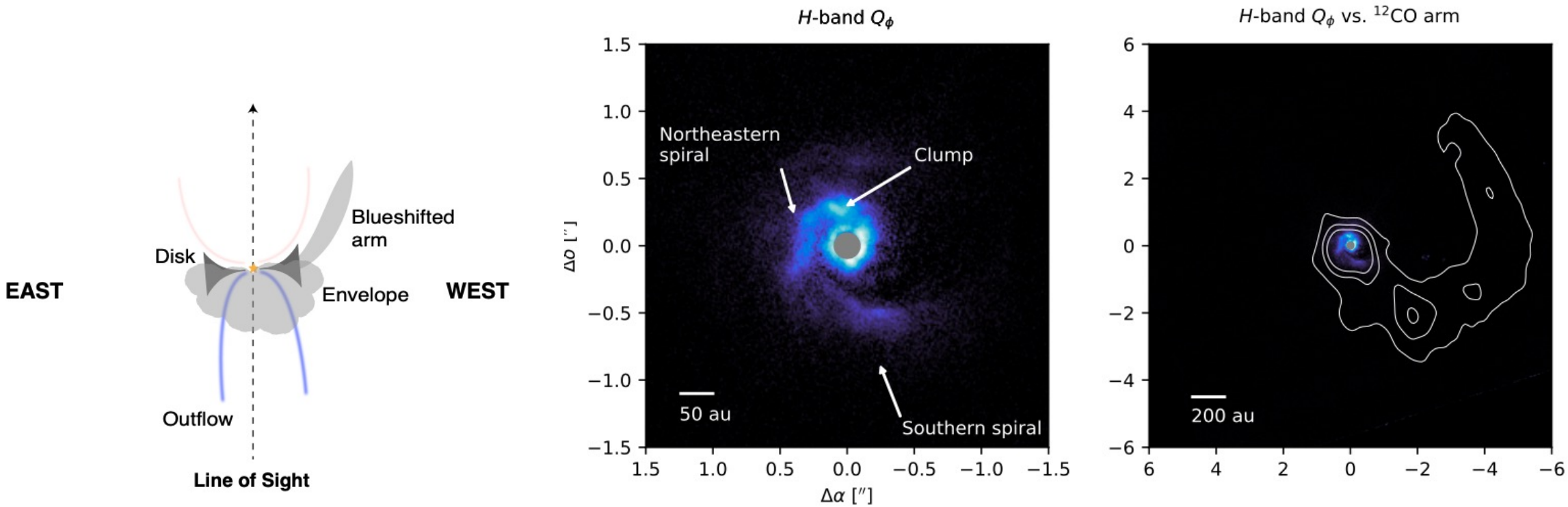
EAST
WEST
Disk
Blueshifted arm
Envelope
Outflow
Line of Sight
H-band Q_ϕ
Northeastern spiral
Clump
Southern spiral
50 au
$\Delta\delta$ [″]
$\Delta\alpha$ [″]
H-band Q_ϕ vs. ^{12}CO arm
200 au

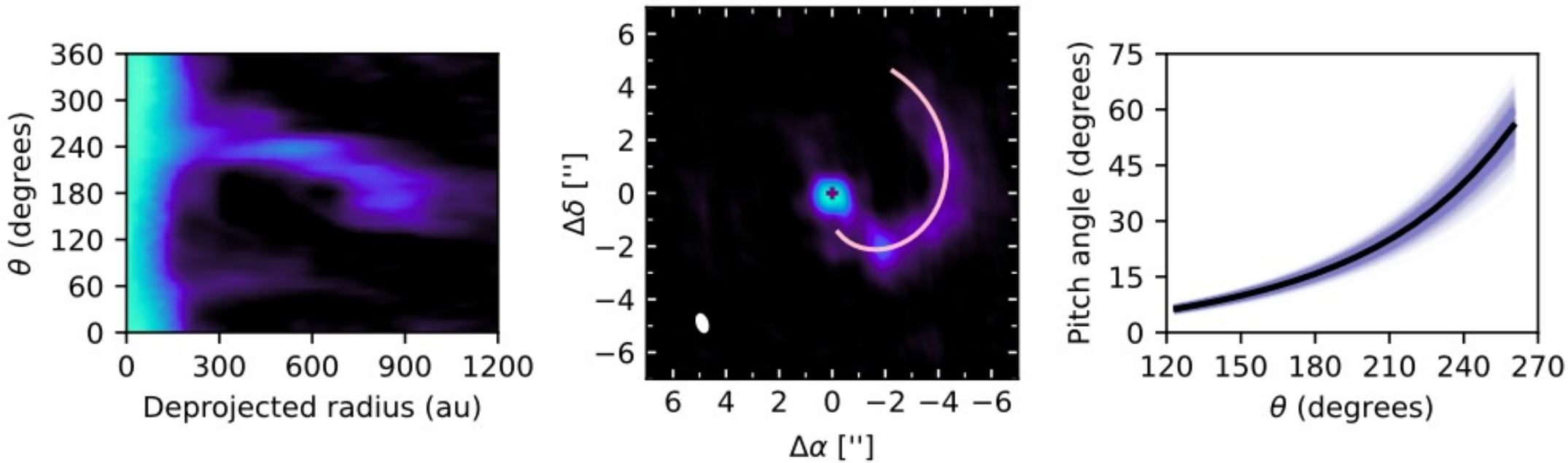
θ (degrees)
360
300
240
180
120
60
0
0
300
600
900
1200
Deprojected radius (au)
Δδ ['']
6
4
2
0
−2
−4
−6
6
4
2
0
−2
−4
−6
Δα ['']
Pitch angle (degrees)
75
60
45
30
15
0
120
150
180
210
240
270
θ (degrees)

28. **Reflections on nebulae around young stars: A systematic search for late-stage infall of material onto Class II disks**

Aashish Gupta, Anna Miotello, Carlo F. Manara, Jonathan P. Williams, Stefano Facchini, Giacomo Beccari, Til Birnstiel, Christian Ginski, Alvaro Hacar, Michael Küffmeier, Leonardo Testi, Lukasz Tychoniec, Hsi-Wei Yen

★ Context. While it is generally assumed that Class II sources evolve largely in isolation from their environment, many still lie close to molecular clouds and may continue to interact with them. This may result in late accretion of material onto the disk that can significantly influence disk processes and planet formation. Aims. In order to systematically study late infall of gas onto disks, we identify candidate Class II sources in close vicinity to a reflection nebula (RN) that may be undergoing this process. Methods. First we targeted Class II sources with known kilo-au scale gas structures - possibly due to late infall of material - and we searched for RNe in their vicinity in optical and near-infrared images. Second, we compiled a catalogue of Class II sources associated with RNe and looked for the large-scale CO structures in archival ALMA data. Using the catalogues of protostars and RNe, we also estimated the probability of Class II sources interacting with surrounding material. Results. All of the sources with large-scale gas structures also exhibit some reflection nebulosity in their vicinity. Similarly, at least five Class II objects associated with a prominent RNe, and for which adequate ALMA observations are available, were found to have spirals or stream-like structures which may be due to late infall. We report the first detection of these structures around S CrA. Conclusions. Our results suggest that a non-negligible fraction of Class II disks in nearby star-forming regions may be associated with RNe and could therefore be undergoing late accretion of gas. Surveys of RNe and kilo-au scale gas structures around Class II sources will allow us to better understand the frequency and impact of late-infall phenomena.

Class II段階でのlate infallの効果を調べるべく、
反射星雲内のClass II円盤のCO輝線分布をALMAアーカイブデータで調査

渦状腕やストリーマーのような構造を発見。

http://arxiv.org/abs/2301.02994v1

COでlarge scale構造が知られている天体

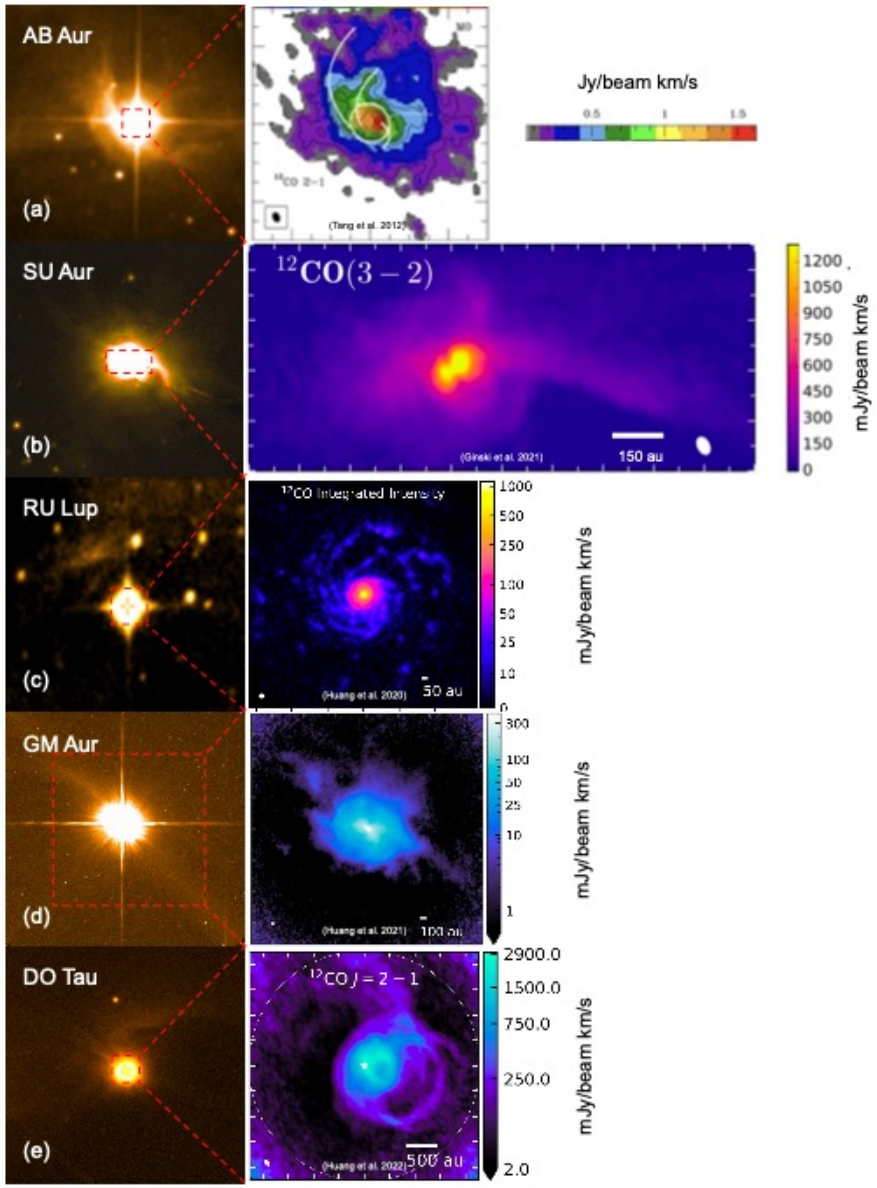

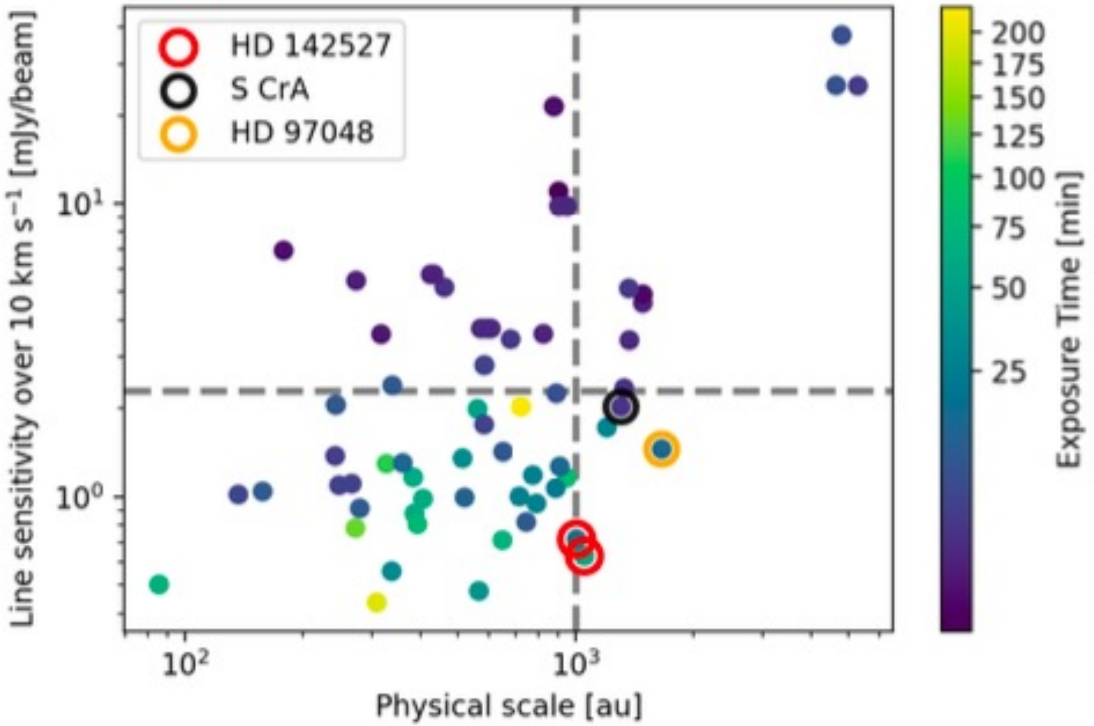

反射星雲近くにある天体

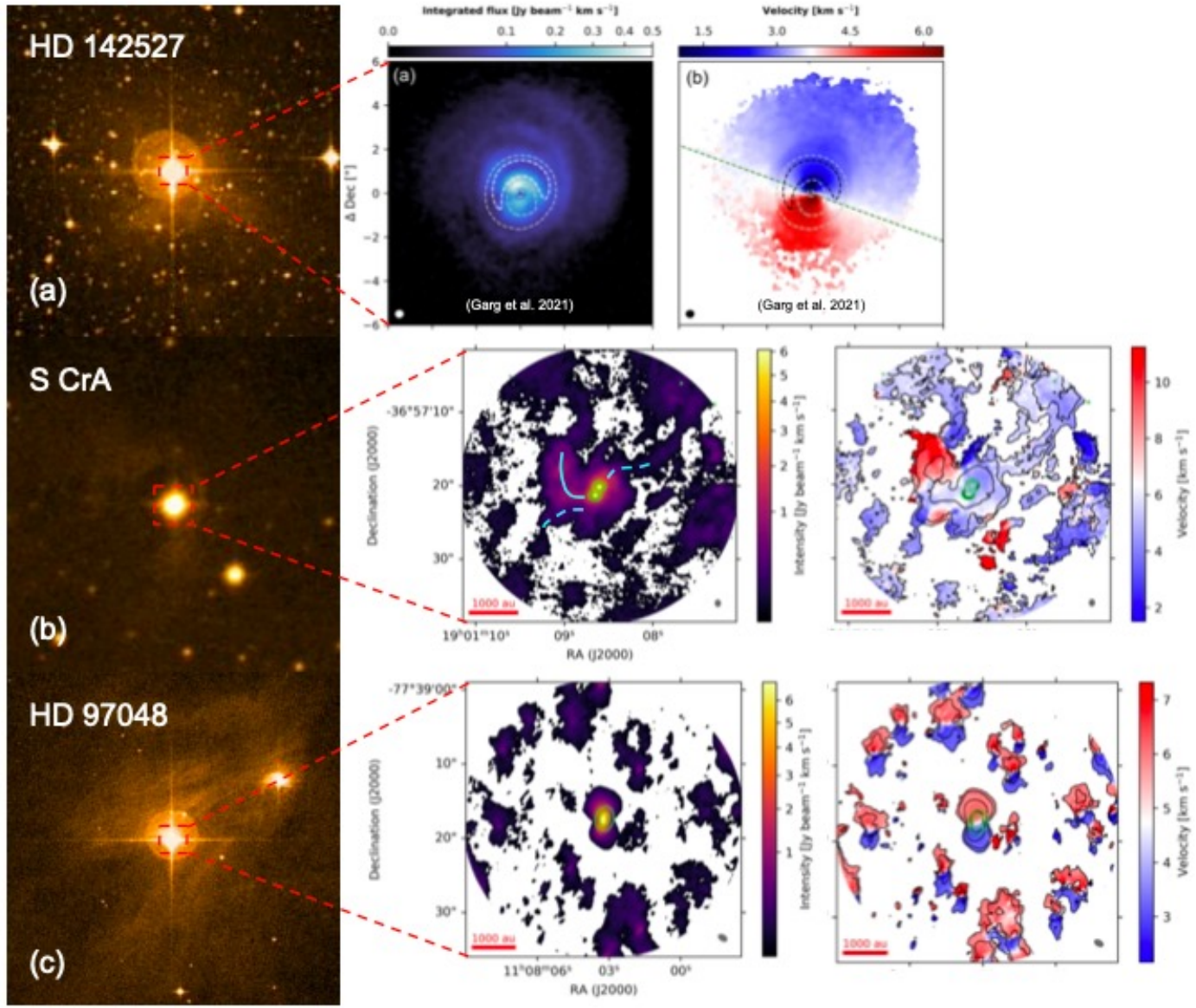

Streamer?

18. What does a typical full-disc around a post-AGB binary look like? – Radiative transfer models reproducing PIONIER, GRAVITY, and MATISSE data

A. Corporaal, J. Kluska, H. Van Winckel, D. Kamath, M. Min ★ (abridged) Stable circumbinary discs around evolved post-Asymptotic Giant branch (post-AGB) binary systems show many similarities with protoplanetary discs around young stellar objects. These discs can provide constraints on both binary evolution and the formation of macrostructures within circumstellar discs. Here we focus on one post-AGB binary system: IRAS08544-4431. We aim to refine the physical model of IRAS08544-4431 with a radiative transfer treatment and continue the near-infrared and mid-infrared interferometric analysis covering the H-, K-, L-, and N-bands. We aim to capture the previously detected amount of over-resolved flux and the radial intensity profile at and beyond the inner dust disc rim to put constraints on the physical processes in the inner disc regions. We used a Monte Carlo radiative transfer code to investigate the physical structure of the disc by reproducing both the photometry and the multi-wavelength infrared interferometric data set. We developed a strategy to identify the models which perform best to reproduce our data set. We found a family of models that successfully fit the infrared photometric and interferometric data in all bands. Some over-resolved flux component was recovered in all bands but the optimised models still fall short to explain all the over-resolved flux. This suggests that another dusty structure within the system plays a role. Multi-wavelength infrared interferometric observations of circumstellar discs allow to study the inner disc regions in unprecedented detail. The refined physical models can reproduce most of the investigated features, including the photometric characteristics, the radial extent, and the overall shape of the visibility curves. Our multi-wavelength interferometric observations combined with photometry show that the disc is similar to protoplanetary discs with similar dust masses and efficient dust growth.

19. ## Climbing the Cliffs: Classifying YSOs in the Cosmic Cliffs using a ML Approach with JWST Data

B. L. Crompvoets, H. Teimoorinia, J. Di Francesco ★ The James Webb Space Telescope (JWST) observed a section of the star forming region NGC 3324 during its Early Release Observations. We make use of the Probabilistic Random Forest machine learning model to identify YSOs within the field of view. We build a matched catalog from photometry data products available on the Mikulski Space Telescope Archive and retrieve 8632 objects, of which Spitzer previously detected 458. We use previously classified data from Spitzer to train on a sample of the Webb data. We retrieve a total of 72 YSO candidates within the data field, 52 of which are only visible with JWST.

20. Dynamics of dust grains in turbulent molecular clouds. Conditions for decoupling and limits of different numerical implementations

Benoît Commerçon, Ugo Lebreuilly, Daniel J. Price, Francesco Lovascio, Guillaume Laibe, Patrick Hennebelle

★ Dust grain dynamics in molecular clouds is regulated by its interplay with supersonic turbulent gas motions. The conditions under which dust grains decouple from the dynamics of gas remain poorly constrained. We first aim to investigate the critical dust grain size for dynamical decoupling, using both analytical predictions and numerical experiments. Second, we aim to set the range of validity of two fundamentally different numerical implementations for the evolution of dust and gas mixtures in turbulent molecular clouds. We carried out a suite of numerical experiments using two different schemes. First, we used a monofluid formalism in the terminal velocity approximation (TVA) on a Eulerian grid. Second, we used a two-fluid scheme, in which the dust dynamics is handled with Lagrangian super-particles, and the gas dynamics on a Eulerian grid. The monofluid results are in good agreement with the theoretical critical size for decoupling. We report dust dynamics decoupling for Stokes number St>0.1, that is, dust grains of $s > 4$ μm in size. We find that the TVA is well suited for grain sizes of 10 μm in molecular clouds, in particular in the densest regions. However, the maximum dust enrichment measured in the low-density material where St>1 is questionable. In the Lagrangian dust experiments, we show that the results are affected by the numerics for all dust grain sizes. At St«1, the dust dynamics is largely affected by artificial trapping in the high-density regions, leading to spurious variations of the dust concentration. At St>1, the maximum dust enrichment is regulated by the grid resolution used for the gas dynamics. The results of previous similar numerical work should therefore be revisited with respect to the limitations we highlight in this study. Dust enrichment of submicron dust grains is unlikely to occur in the densest parts of molecular clouds.

21. Mercury's formation within the Early Instability Scenario

Matthew S. Clement, John E. Chambers, Nathan A. Kaib, Sean N. Raymond, Alan P. Jackson ★ The inner solar system's modern orbital architecture provides inferences into the epoch of terrestrial planet formation; a 100 Myr time period of planet growth via collisions with planetesimals and other proto-planets. While classic numerical simulations of this scenario adequately reproduced the correct number of terrestrial worlds, their semi-major axes and approximate formation timescales, they struggled to replicate the Earth-Mars and Venus-Mercury mass ratios.

In a series of past independent investigations, we demonstrated that Mars' mass is possibly the result of Jupiter and Saturn's early orbital evolution, while Mercury's diminutive size might be the consequence of a primordial mass deficit in the region. Here, we combine these ideas in a single modeled scenario designed to simultaneously reproduce the formation of all four terrestrial planets and the modern orbits of the giant planets in broad strokes. By evaluating our Mercury analogs' core mass fractions, masses, and orbital offsets from Venus, we favor a scenario where Mercury forms through a series of violent erosive collisions between a number of Mercury-mass embryos in the inner part of the terrestrial disk. We also compare cases where the gas giants begin the simulation locked in a compact 3:2 resonant configuration to a more relaxed 2:1 orientation and find the former to be more successful. In 2:1 cases, the entire Mercury-forming region is often depleted due to strong sweeping secular resonances that also tend to overly excite the orbits of Earth and Venus as they grow. While our model is quite successful at replicating Mercury's massive core and dynamically isolated orbit, the planets' low mass remains extremely challenging to match. Finally, we discuss the merits and drawbacks of alternative evolutionary scenarios and initial disk conditions.

22. A Herschel study of the high-mass protostar IRAS20126+4104

R. Cesaroni, F. Faustini, D. Galli, A. Lorenzani, S. Molinari, L. Testi ★ We performed Herschel observations of the continuum and line emission from the high-mass star-forming region IRAS20126+4104, which hosts a well-studied B-type (proto)star powering a bipolar outflow and is associated with a Keplerian circumstellar disk. The continuum images at six wavelengths allowed us to derive an accurate estimate of the bolometric luminosity and mass of the molecular clump enshrouding the disk. The same region has been mapped in 12 rotational transitions of carbon monoxide, which were used in synergy with the continuum data to determine the temperature and density distribution inside the clump and improve upon the mass estimate. The maps of two fine structure oxygen far-IR lines were used to estimate the volume density of the shocked region at the surface of the southern lobe of the outflow and the mass-loss rate. Our findings lend further support to the scenario previously proposed by various authors, confirming that at the origin of the bolometric luminosity and bipolar outflow from IRAS20126+4104 is a B-type star located at the centre of the Keplerian disk.

23. A Complete HCN Survey of the Perseus Molecular Cloud

T. M. Dame, Charles J. Lada ★ We present a survey of the Perseus molecular cloud in the J = 1→0 transition of HCN, a widely used tracer of dense molecular gas. The survey was conducted with the CfA 1.2 m telescope, which at 89 GHz has a beam width of 11' and a spectral resolution of 0.85 km s^{-1}. A total of 8.1 deg^2 was surveyed on a uniform 10' grid to a sensitivity of 14 mK per channel. The survey was compared with similar surveys of CO and dust in order to study and calibrate the HCN line as a dense gas tracer. We find the HCN emission to extend over a considerable fraction of the cloud. We show that the HCN intensity remains linear with H_2 column density well into the regime where the CO line saturates. We use radiative transfer modeling to show that this likely results from subthermal excitation of HCN in a cloud where the column and volume densities of H_2 are positively correlated. To match our HCN observations the model requires an exponential decrease in HCN abundance with increasing extinction, consistent with HCN depletion onto grains. The modeling also reveals that the mean volume density of H_2 in the HCN emitting regions is $\sim 10^4$ cm^{-3}, well below the HCN critical density. For the first time, we obtain a direct measurement of the ratio of dense gas mass to HCN luminosity for an entire nearby molecular cloud: $\alpha(HCN) = 92$ $M_\odot/(K\ km\ s^{-1}\ pc^2)$.

24. Twisted magnetic field in star formation processes of L1521 F revealed by submillimeter dual band polarimetry using James Clerk Maxwell Telescope

Sakiko Fukaya, Hiroko Shinnaga, Ray S. Furuya, Kohji Tomisaka, Masahiro N. Machida, Naoto Harada ★

Understanding the initial conditions of star formation requires both observational studies and theoretical works taking into account the magnetic field, which plays an important role in star formation processes. Herein, we study the young nearby dense cloud core L1521 F ($n(\mathrm{H_2}) \sim 10^{4-6}$ cm^{-3}) in the Taurus Molecular Cloud. This dense core hosts a 0.2 $M_\odot$ protostar, categorized as a Very Low Luminosity Objects with complex velocity structures, particularly in the vicinity of the protostar. To trace the magnetic field within the dense core, we conducted high sensitivity submillimeter polarimetry of the dust continuum at λ= 850 μm and 450 μm using the POL-2 polarimeter situated in front of the SCUBA-2 submillimeter bolometer camera on James Clerk Maxwell Tetescope. This was compared with millimeter polarimetry taken at λ= 3.3 mm with ALMA. The magnetic field was detected at λ= 850 μm in the peripheral region, which is threaded in a north-south direction, while the central region traced at λ= 450 μm shows a magnetic field with an east-west direction, i.e., orthogonal to that of the peripheral region. Magnetic field strengths are estimated to be ∼70 μG and 200 μG in the peripheral- and central-regions, respectively, using the Davis-Chandrasekhar-Fermi method. The resulting mass-to-flux ratio of 3 times larger than that of magnetically critical state for both regions indicates that L1521 F is magnetically supercritical, i.e., gravitational forces dominate over magnetic turbulence forces. Combining observational data with MHD simulations, detailed parameters of the morphological properties of this puzzling object are derived for the first time.

25. Forbidden emission lines in protostellar outflows and jets with MUSE

Lizxandra Flores-Rivera, Mario Flock, Nicolás Kurtovic, Bernd Husemann, Andrea Banzatti, Simon C. Ringqvist, Sebastian Kamann, André Müller, Christian Fendt, Rebeca Garcia Lopez, Gabriel-Dominique Marleau, Thomas Henning, Carlos Carrasco-Gonzalez, Roy van Boekel, Miriam Keppler, Ralf Launhardt, Yuhiko Aoyama ★

Forbidden emission lines in protoplanetary disks are a key diagnostic in studies of the evolution of the disk and the host star. We report spatially resolved emission lines, [OI] 6300, 6363, [NII] 6548, 6583, Hα, and [SII] 6716, 6730 Angstrom that are believed to be associated with jets and magnetically driven winds in the inner disks. Observations were carried out with the optical integral field spectrograph of the Multi Unit Spectroscopic Explorer (MUSE), at the Very Large Telescope (VLT). With a resolution of 0.025 X 0.025 arcsec^2, we aim to derive the position angle of the outflow/jet ($PA_{outflow/jet}$) that is connected with the inner disk. The forbidden emission lines analyzed here have their origin at the inner parts of the protoplanetary disk. From the maximum intensity emission along the outflow/jet in DL Tau, CI Tau, DS Tau, IP Tau, and IM Lup, we were able to reliably measure the $PA_{outflow/jet}$ for most of the identified lines. We found that our estimates agree with PA_{dust} for most of the disks. These estimates depend on the signal-to-noise level and the collimation of the outflow (jet). The outflows/jets in CIDA 9, GO Tau, and GW Lup are too compact for a $PA_{outflow/jet}$ to be estimated. Based on our kinematics analysis, we confirm that DL Tau and CI Tau host a strong outflow/jet with line-of-sight velocities much greater than 100 km s^{-1}, whereas DS Tau, IP Tau, and IM Lup velocities are lower and their structures encompass low-velocity components to be more associated with winds. Our estimates for the mass-loss rate, $\dot{M}_{loss}$, range between (1.1-6.5)X10^{-7}-10^{-8} $M_\odot$ yr^{-1} for the disk-outflow/jet systems analyzed here. The outflow/jet systems analyzed here are aligned within around 1 degree between the inner and outer disk. Further observations are needed to confirm a potential misalignment in IM Lup.

26. A High-resolution Optical Survey of Upper Sco: Evidence for Coevolution of Accretion and Disk Winds

Min Fang, Ilaria Pascucci, Suzan Edwards, Uma Gorti, Lynne A. Hillenbrand, John M. Carpenter ★ Magnetohydrodynamic (MHD) and photoevaporative winds are thought to play an important role in the evolution and dispersal of planet-forming disks. Here, we analyze high-resolution ($\Delta v \sim 7$ kms^{-1}) optical spectra from a sample of 115 T Tauri stars in the $\sim 5-10$ Myr Upper Sco association and focus on the [O I]λ6300 and Hα lines to trace disk winds and accretion, respectively. Our sample covers a large range in spectral type and we divide it into Warm (G0-M3) and Cool (later than M3) to facilitate comparison with younger regions. We detect the [O I]λ6300 line in 45 out of 87 upper sco sources with protoplanetary disks and 32 out of 45 are accreting based on Hα profiles and equivalent widths. All [O I] λ6300 Upper Sco profiles have a low-velocity (centroid < -30 kms^{-1}, LVC) emission and most (36/45) can be fit by a single Gaussian (SC). The SC distribution of centroid velocities and FWHMs is consistent with MHD disk winds. We also find that the Upper Sco sample follows the same accretion luminosity−LVC [O I]λ6300 luminosity relation and the same anti-correlation between SC FWHM and WISE W3-W4 spectral index as the younger samples. These results indicate that accretion and disk winds coevolve and that, as inner disks clear out, wind emission arises further away from the star. Finally, our large spectral range coverage reveals that Cool stars have larger FWHMs normalized by stellar mass than Warm stars indicating that [O I]λ6300 emission arises closer in towards lower mass/lower luminosity stars.

27. **The active weak-line T Tauri star LkCa 4 observed with SPIRou and TESS**

Benjamin Finociety, Jean-François Donati, Konstantin Grankin, Jérôme Bouvier, Silvia Alencar, François Ménard, Tom P. Ray, Ágnes Kóspál, the SLS consortium

★ We report results of a spectropolarimetric and photometric monitoring of the weak-line T Tauri star LkCa 4 within the SPIRou Legacy Survey large programme, based on data collected with SPIRou at the Canada-France-Hawaii Telescope and the TESS space probe between October 2021 and January 2022. We applied Zeeman-Doppler Imaging to our spectropolarimetric and photometric data to recover a surface brightness distribution compatible with TESS photometry, as well as the large-scale magnetic topology of the star. As expected from the difference in wavelength between near-infrared and optical data, the recovered surface brightness distribution is less contrasted than the previously published one based on ESPaDOnS data, but still features mid-latitude dark and bright spots. The large-scale magnetic field is consistent in shape and strength with the one derived previously, with a poloidal component resembling a 2.2 kG dipole and a toroidal component reaching 1.4 kG and encircling the star at the equator. Our new data confirm that the surface differential rotation of LkCa 4 is about 10 times weaker than that of the Sun, and significantly different from zero. Using our brightness reconstruction and Gaussian Process Regression, we were able to filter the radial velocity activity jitter down to a precision of 0.45 and 0.38 km s^{-1} (from an amplitude of 6.10 km s^{-1}), respectively, yielding again no evidence for a close-in massive planet orbiting the star.

30. Has the dust clump in the debris disk of Beta Pictoris moved?

Yinuo Han, Mark C. Wyatt, William R. F. Dent ★ The edge-on debris disk of the nearby young star Beta Pictoris shows an unusual brightness asymmetry in the form of a clump. The clump has been detected in both the mid-IR and CO and its origin has so far remained uncertain. Here we present new mid-IR observations of Beta Pic to track any motion of the dust clump. Together with previous observations, the data span a period of 12 years. We measured any projected displacement of the dust clump over the 12-yr period to be $0.2^{+1.3}_{-1.4}$ au away from the star based on the median and 1σ uncertainty, and constrain this displacement to be <11 au at the 3σ level. This implies that the observed motion is incompatible with Keplerian motion at the 2.8σ level. It has been posited that a planet migrating outwards may trap planetesimals into a 2:1 resonance, resulting in the observed clump at pericentre of their orbits that trails the planet. The observed motion is also incompatible with such resonant motion at the 2.6σ level. While Keplerian motion and resonant motion is still possible, the data suggest that the dust clump is more likely stationary. Such a stationary dust clump could originate from the collision or tidal disruption of a planet-sized body, or from secular perturbations due to a planet that create regions with enhanced densities in the disk.

31. X-Shooter Survey of Young Intermediate Mass Stars – I. Stellar Characterization and Disc Evolution

Daniela P. Iglesias, Olja Panić, Mario van den Ancker, Monika G. Petr-Gotzens, Lionel Siess, Miguel Vioque, Ilaria Pascucci, René Oudmaijer, James Miley ★ Intermediate mass stars (IMSs) represent the link between low-mass and high-mass stars and cover a key mass range for giant planet formation. In this paper, we present a spectroscopic survey of 241 young IMS candidates with IR-excess, the most complete unbiased sample to date within 300 pc. We combined VLT/X-Shooter spectra with BVR photometric observations and Gaia DR3 distances to estimate fundamental stellar parameters such as Teff, mass, radius, age, and luminosity. We further selected those stars within the intermediate mass range 1.5 <= Mstar/Msun <= 3.5 and discarded old contaminants. We used 2MASS and WISE photometry to study the IR-excesses of the sample, finding 92 previously unidentified stars with IR-excess. We classified this sample into 'protoplanetary', 'hybrid candidates' and 'debris' discs based on their observed fractional excess at 12microns, finding a new population of 17 hybrid disc candidates. We studied inner disc dispersal timescales for $\lambda < 10\mu$m and found very different trends for IMSs and low mass stars (LMSs). IMSs show excesses dropping fast during the first 6 Myrs independently of the wavelength, while LMSs show consistently lower fractions of excess at the shortest wavelengths and increasingly higher fractions for longer wavelengths, with slower dispersal rates. In conclusion, this study demonstrates empirically that IMSs dissipate their inner discs very differently than LMSs, providing a possible explanation for the lack of short period planets around IMSs.

32. A rich molecular chemistry in the gas of the IC 348 star cluster of the Perseus Molecular Cloud

Susana Iglesias-Groth, Martina Marin-Dobrincic ★
We present Spitzer 10-34 μm spectroscopic observations of the diffuse gas in the inner region of the star-forming region IC 348 of the Perseus Molecular Cloud. We find evidence for the strongest mid-IR bands of common molecules as H_2, OH, H_2O,CO_2 and NH_3 and of several carbonaceous molecules which may play an important role in the production of more complex hydrocarbons: HCN, C_2H_2, C_4H_2, HC_3N, HC_5N, C_2H_6, C_6H_2, C_6H_6. The excitation diagram of H_2 reveals the presence of warm gas (270 +- 30 K) at the observed locations. Assuming this temperature, the derived abundances of CO_2 and NH_3 relative to H_2 are 10^{-8} and 10^{-7}, respectively. From the water lines we obtain an abundance of order 10^{-6} and higher gas temperatures. The abundances derived for HCN and C_2H_2, key molecules in the development of prebiotic building blocks, are of order 10^{-7} and 10^{-9}, respectively. More complex molecules such as PAHs and the fullerenes C_{60} and C_{70} are also present. IC 348 appears to be very rich and diverse in molecular content. The JWST spectroscopic capabilities may provide details on the spatial distribution of all these molecules and extend the present search to more complex hydrocarbons.